Available online at www.sciencedirect.com
SCIENCE DIRECT®
International Journal of Thermal Sciences 44 (2005) 915–925
International Journal of Thermal Sciences
www.elsevier.com/locate/ijts

Convective behaviour of a uniformly Joule-heated liquid pool in a rectangular cavity

G. Sugilal [a,*], P.K. Wattal [a], K. Iyer [b]

[a] *Back-End Technology Development Division, Bhabha Atomic Research Centre, Mumbai-400 085, India*
[b] *Department of Mechanical Engineering, Indian Institute of Technology Bombay, Mumbai-400 076, India*

Received 11 October 2004; received in revised form 7 March 2005; accepted 7 March 2005

Available online 23 May 2005

Abstract

A two-dimensional mathematical model has been developed to study the interaction between gravitational body force and self-induced electromagnetic body force in a Joule-heated liquid pool in a rectangular cavity, with an aspect ratio of 2. The Joule heating of the liquid pool in the cavity is accomplished by passing a large alternating current employing a pair of plate electrodes immersed in the liquid. The electrode surfaces are assumed to be isopotential and rest of the boundaries is treated as electrically insulated. The upper boundary of the liquid pool is an isothermal boundary while the rest of the boundaries are assumed to be thermally insulated. The present study investigates the convective behaviour of different liquids under Joule heating. Numerical simulations have been carried out employing Boussinesq fluids for Rayleigh numbers up to 2.5×10^5 and Hartmann numbers up to 4×10^7. This study shows that the heat transfer in the uniformly Joule-heated liquid is governed by the gravitational body force when $Ha^2 Pr/\sqrt{Ra} < 120$ and by the self-induced electromagnetic body force when $Ha^2 Pr/Ra > 100$. It also indicates that the thermal field is strongly dependent on Pr in electromagnetically driven flows while Pr has negligible effect on temperature field in thermally driven flows for $10^3 \geqslant Pr \geqslant 10$. Heat transfer correlations for thermally driven flows, electromagnetically driven flows and combined flows are also presented.

Keywords: Joule heating; Internal heat generation; Natural convection; Magnetohydrodynamic flow; Heat transfer

1. Introduction

The principle of Joule heating is extensively made use of in the electrothermal industries to give rise to elevated process temperatures. For example, Joule heating is used for melting glasses in electric glass melters and for heating molten slag in electro-slag remelting process applied in the steel industry. The above electrothermal processes employ either direct current or low frequency, alternating currents for heating the process medium, which is in liquid state placed between a pair of electrodes.

Physical phenomena taking place inside Joule-heated liquid pools are quite complex and interrelated. The heat transfer in the liquid pool is governed by the natural convection caused by the body forces generated on account of Joule heating. Two types of body forces prevail in an electrically conducting liquid under Joule heating. These are the *gravitational body force* due to the non-uniform temperature field and the *electromagnetic body force* due to the interaction between self-induced magnetic field and moving charge carriers in the liquid. The convective behaviour of the liquid pool under Joule heating depends strongly on the interaction between the two body forces.

Mathematical models have been developed by various researchers to study the convective behaviour of liquids under Joule heating [1–5]. Models developed for predicting the flow field and the temperature distribution inside the

* Corresponding author. Tel.: +91 22 25591074; fax: +91 22 25505185.
E-mail address: gsugilal@gmail.com (G. Sugilal).

1290-0729/$ – see front matter
doi:10.1016/j.ijthermalsci.2005.03.012

Nomenclature

A	magnetic vector potential	$V\cdot s\cdot m^{-1}$
B	magnetic flux density vector	$Wb\cdot m^{-2}$
D	electric flux density	$C\cdot m^{-2}$
E	electric field intensity	$V\cdot m^{-1}$
g	gravitational acceleration vector	$m\cdot s^{-2}$
g	acceleration due to gravity 9.81	$m\cdot s^{-2}$
h	heat transfer coefficient	$W\cdot m^{-2}\cdot K^{-1}$
H	magnetic field strength	$A\cdot m^{-1}$
J	electric current density	$A\cdot m^{-2}$
k	thermal conductivity	$W\cdot m^{-1}\cdot K^{-1}$
L	vertical dimension of cavity	m
p	excess pressure over static pressure	$N\cdot m^{-2}$
r	position vector	m
t	time	s
T	temperature	K
u	velocity along x direction	$m\cdot s^{-1}$
V	velocity vector	$m\cdot s^{-1}$
w	velocity along the z direction	$m\cdot s^{-1}$
W	horizontal dimension of cavity	m
x, y, z	Cartesian coordinates	m

Greek symbols

α	thermal diffusivity	$m^2\cdot s^{-1}$
β	coefficient of volumetric expansion	K^{-1}
φ	electric scalar potential	V
μ	magnetic permeability	$H\cdot m^{-1}$
ν	kinematic viscosity	$m^2\cdot s^{-1}$
ρ	density	$kg\cdot m^{-3}$
σ	electrical conductivity	$mho\cdot m^{-1}$
ω	angular frequency of current	$rad\cdot s^{-1}$
∇	gradient operator	m^{-1}
∇^2	Laplacian operator	m^{-2}
Δ	difference of a quantity	

Superscript

$'$	dummy variable

Subscript

0	reference value
avg	average value
max	maximum value
x, y, z	component of a vector quantity

Dimensionless quantities

$\widetilde{\mathbf{A}}$	magnetic vector potential, $\mathbf{A}W/\sigma\mu\varphi_0 L^2$
$\widetilde{\mathbf{B}}$	magnetic flux density, $\mathbf{B}W/\sigma\mu\varphi_0 L$
$\widetilde{\mathbf{E}}$	electric field intensity, $\mathbf{E}W/\varphi_0$
$\widetilde{\mathbf{J}}$	electric current density, $\mathbf{J}W/\sigma\varphi_0$
$\tilde{p}$	pressure, $pL^2/\rho\nu^2$
$\widetilde{T}$	temperature, $2(T-T_0)kW^2/\sigma\varphi_0^2 L^2$
$\tilde{u}, \tilde{w}$	x- and z-components of $\widetilde{\mathbf{V}}$
$\widetilde{\mathbf{V}}$	velocity vector, $\mathbf{V}L/\nu$
$\tilde{x}$	Cartesian coordinate in x direction, x/L
$\tilde{z}$	Cartesian coordinate in z direction, z/L
$\tilde{\varphi}$	electric scalar potential, φ/φ_0
$\widetilde{\nabla}$	gradient operator, ∇L
$\widetilde{\nabla}^2$	Laplacian operator, $\nabla^2 L^2$

Dimensionless numbers

a	aspect ratio, W/L
Ha	Hartmann number, $J_0 L^2\sqrt{\mu/\rho_0\nu^2} = L\sigma\varphi_0\sqrt{\mu/\rho_0\nu^2 a^2}$
Nu_{avg}	average Nusselt number, $2/\frac{1}{a}\int_0^a \widetilde{T}\,\mathrm{d}\tilde{x}$
N_f	square of the ratio of L to the electromagnetic wavelength, $\omega\mu\sigma L^2$
N_{Rem}	magnetic Reynolds number, $\sigma\mu L V_0 = \sigma\mu\nu$
Pr	Prandtl number, ν/α
Ra	Rayleigh number, $L^3 g\beta\Delta T_0/\nu\alpha = L^3 g\beta\sigma\varphi_0^2/2k\alpha\nu a^2$

electro-slag remelting furnace assume that the gravitational body force can be neglected when compared with the electromagnetic body force [1,2]. On the other hand, the electromagnetic body force is ignored in the models for the electric glass melters [3–5]. Thus, it is evident from the literature that physical properties of electrically conducting liquids strongly govern their convective behaviour under Joule-heating. The present study investigates the convective behaviour of different electrically conducting liquids ranging from molten metal to molten glass. Main aim of this study is to identify the conditions under which each one of these two body forces prevailing in a Joule-heated liquid pool dominates the other. It also characterises convective behaviour of thermally driven flows, electromagnetically driven flows and combined flows in a Joule-heated liquid pool. Heat transfer correlations for these three types of flow are also presented.

2. Governing equations and boundary conditions

Mathematical model to describe the state of an electrically conducting liquid pool in a cavity involves model equations for fluid flow, heat transfer and Maxwell's equations describing the electromagnetic field.

2.1. Electromagnetic field

The Maxwell's equations describing the electromagnetic fields prevailing in a Joule-heated liquid pool can be written as

$$\nabla\times\mathbf{E} = -\frac{\partial\mathbf{B}}{\partial t} \tag{1}$$

$$\nabla\times\mathbf{H} = \mathbf{J} + \frac{\partial\mathbf{D}}{\partial t} \tag{2}$$

$$\nabla \cdot \mathbf{B} = 0 \tag{3}$$

Further, the equation of electric charge continuity in a Joule-heated liquid pool can be expressed as

$$\nabla \cdot \mathbf{J} = 0 \tag{4}$$

In addition to the above equations, constitutive relations as given by Eqs. (5) and (6) exist. Relation stated in Eq. (6) is known as Ohm's Law

$$\mathbf{B} = \mu \mathbf{H} \tag{5}$$

$$\mathbf{J} = \sigma(\mathbf{E} + \mathbf{V} \times \mathbf{B}) \tag{6}$$

At low frequencies, i.e. when the rates of time variation are sufficiently slow, the displacement-current ($\partial \mathbf{D}/\partial t$) can be neglected. For such cases, Eq. (2) can be simplified and re-written as Eq. (7) using Eq. (5).

$$\nabla \times \mathbf{B} = \mu \mathbf{J} \tag{7}$$

Upon combining Eqs. (1), (6) and (7) the following expression is obtained:

$$\nabla \times \nabla \times \mathbf{E} = -\mu \frac{\partial[\sigma(\mathbf{E} + \mathbf{V} \times \mathbf{B})]}{\partial t} \tag{8}$$

For the sinusoidal variation of an applied electric field, the electric and magnetic fields can respectively be represented by Eq. (9) and (10).

$$\mathbf{E} = \widehat{\mathbf{E}}\, e^{j\omega t} \tag{9}$$

$$\mathbf{B} = \widehat{\mathbf{B}}\, e^{j\omega t} \tag{10}$$

where $\widehat{\mathbf{B}}$ and $\widehat{\mathbf{E}}$ are complex amplitude of the phasors $\mathbf{E}$ and $\mathbf{B}$, ω is frequency and $j = \sqrt{-1}$. For a steady velocity field, Eqs. (8)–(10) can be combined to get Eq. (11)

$$\nabla \times \nabla \times \widehat{\mathbf{B}} = -j\omega\mu\sigma\left(\widehat{\mathbf{B}} + \mathbf{V} \times \widehat{\mathbf{E}}\right) \tag{11}$$

which can be re-written in the following dimensionless form, assuming that electrical conductivity and magnetic permeability remain constant:

$$\widetilde{\nabla} \times \widetilde{\nabla} \times \widetilde{\mathbf{E}} = -jN_f\left[\widetilde{\mathbf{E}} + N_{\mathrm{Rem}}\widetilde{\mathbf{V}} \times \widetilde{\mathbf{B}}\right] \tag{12}$$

The dimensionless quantity N_f represents the square of the ratio of the length scale to the wavelength of electromagnetic field oscillation and N_{Rem} is the magnetic Reynolds number, which can be defined as the ratio of convective to diffusive transport of electromagnetic field. The values of N_f and N_{Rem} for a typical industrial scale electro-slag remelting unit are of the orders of 10^{-3} and 10^{-4} respectively [1]. These quantities are also typically small for glass melting operations [4]. Under such conditions, the electric field can be regarded as eddy free field and therefore, the same can be expressed in terms of the electric scalar potential as

$$\mathbf{E} = -\nabla\varphi \tag{13}$$

For small magnetic Reynolds numbers, the sluggish hydrodynamic behaviour of the liquid pool has negligible effect on the electromagnetic behaviour. For such cases, Ohm's law stated in Eq. (6) can be simplified as

$$\mathbf{J} = \sigma \mathbf{E} \tag{14}$$

Using Eqs. (13) and (14) in Eq. (4), the charge continuity equation can be re-written as

$$\nabla \cdot [\sigma \nabla\varphi] = 0 \tag{15}$$

which takes the following dimensionless form when electrical conductivity is constant:

$$\widetilde{\nabla}^2\tilde{\varphi} = 0 \tag{16}$$

The dimensionless form of the Ohm's Law given by Eq. (14) is

$$\widetilde{\mathbf{J}} = -a\widetilde{\nabla}\tilde{\varphi} \tag{17}$$

where dimensionless quantity 'a' is the aspect ratio of the rectangular cavity in the xz-plane.

The magnetic flux density can be obtained by solving Eq. (7), which has a dimensionless form as given by Eq. (18), subject to the constraint given by Eq. (19) which is the dimensionless form of Eq. (3).

$$\widetilde{\nabla} \times \widetilde{\mathbf{B}} = \widetilde{\mathbf{J}} \tag{18}$$

$$\widetilde{\nabla} \cdot \widetilde{\mathbf{B}} = 0 \tag{19}$$

Since there are no externally applied magnetic fields, the magnetic flux density must vanish at infinity. Eq. (19) can be identically satisfied by introducing the magnetic vector potential, $\widetilde{\mathbf{A}}$, defined by

$$\widetilde{\mathbf{B}} = \nabla \times \widetilde{\mathbf{A}} \tag{20}$$

since the divergence of the curl of any vector field is zero. Using the vector identity $\nabla \times (\nabla \times \mathbf{A}) = \nabla(\nabla \cdot \mathbf{A}) - \nabla^2\mathbf{A}$, Eq. (18) and (20) can be combined to obtain

$$\widetilde{\nabla}\left(\widetilde{\nabla} \cdot \widetilde{\mathbf{A}}\right) - \widetilde{\nabla}^2\widetilde{\mathbf{A}} = \widetilde{\mathbf{J}} \tag{21}$$

The vector potential is arbitrary up to the addition of a gradient of any scalar field (ζ), since $\nabla \times (\mathbf{A} + \nabla\zeta) = \nabla \times \mathbf{A}$ as $\nabla \times \nabla\zeta = \mathbf{0}$ for any scalar field. Therefore, ζ can be chosen such that $\nabla \cdot \mathbf{A} = 0$, which is often referred to as fixing the gauge of $\mathbf{A}$ [6]. Then Eq. (21) reduces to

$$\widetilde{\nabla}^2\widetilde{\mathbf{A}} = -\widetilde{\mathbf{J}} \tag{22}$$

Using the Green's function in 3-D space [7], the vector potential can be expressed as

$$\widetilde{\mathbf{A}}[\tilde{\mathbf{r}}] = \frac{1}{4\pi}\iiint \frac{\widetilde{\mathbf{J}}[\tilde{\mathbf{r}}']}{|\tilde{\mathbf{r}} - \tilde{\mathbf{r}}'|^3}\,\mathrm{d}\tilde{\mathbf{r}}' \tag{23}$$

which satisfies the condition $\nabla \cdot \widetilde{\mathbf{A}} = 0$ as $\nabla \cdot \widetilde{\mathbf{J}} = 0$ in the present study. Therefore, the magnetic flux density at position $\tilde{\mathbf{r}}$, i.e. $\widetilde{\mathbf{B}}[\tilde{\mathbf{r}}]$, induced in the liquid pool due to a current density $\widetilde{\mathbf{J}}[\tilde{\mathbf{r}}']$ at position $\tilde{\mathbf{r}}'$ can be expressed, in its dimensionless form, as given by Eq. (24).

$$\widetilde{\mathbf{B}}[\tilde{\mathbf{r}}] = \frac{1}{4\pi}\iiint \frac{\widetilde{\mathbf{J}}[\tilde{\mathbf{r}}'] \times (\tilde{\mathbf{r}} - \tilde{\mathbf{r}}')}{|\tilde{\mathbf{r}} - \tilde{\mathbf{r}}'|^3}\,\mathrm{d}\tilde{\mathbf{r}}' \tag{24}$$

where $d\tilde{\mathbf{r}}'$ denotes the volume element $d\tilde{x}'\,d\tilde{y}'\,d\tilde{z}'$ and $\tilde{\mathbf{r}} = \mathbf{r}/L$ is the dimensionless position vector.

Since this study considers low frequency alternating current sources for Joule heating, the complex amplitudes of the electromagnetic quantities that appear in the above equations can be replaced with the corresponding rms values.

2.2. Fluid flow

Fluid flow in the system is described by the equation of continuity and by the Navier–Stokes equation for momentum. Assuming the model fluid to be incompressible, the equation of continuity can be expressed as

$$\nabla \cdot \mathbf{V} = 0 \tag{25}$$

which can be rewritten in dimensionless form as

$$\widetilde{\nabla} \cdot \widetilde{\mathbf{V}} = 0 \tag{26}$$

Using the Boussinesq approximation, the Navier–Stokes equation for momentum for a steady, laminar flow can be written as

$$\rho(\mathbf{V}\cdot\nabla)\mathbf{V} = -\nabla p + \mu\nabla^2\mathbf{V} + \mathbf{J}\times\mathbf{B} - \rho\beta(T - T_0)\mathbf{g} \tag{27}$$

which can be non-dimensionalised to obtain

$$\left(\widetilde{\mathbf{V}}\cdot\widetilde{\nabla}\right)\widetilde{\mathbf{V}} = -\widetilde{\nabla}\tilde{p} + \widetilde{\nabla}^2\widetilde{\mathbf{V}} + Ha^2\left(\widetilde{\mathbf{J}}\times\widetilde{\mathbf{B}}\right) + \frac{Ra}{Pr}\widetilde{T} \tag{28}$$

In Eq. (28), the third and fourth terms on the right-hand side represent the electromagnetic body force and the gravitational body force respectively.

The dimensionless numbers *Ra*, *Pr* and *Ha* are the Rayleigh number, the Prandtl number and the Hartmann number respectively. It is well known that the Rayleigh number, which is the buoyant force divided by the product of the viscous drag and the rate of heat diffusion, characterises the buoyancy driven natural convection while the Hartmann number governs the magnetohydrodynamic flows. Traditionally, the Hartmann number is defined as $Ha = B_0 L_0\sqrt{\sigma/\rho\nu}$ [8]. This definition is obtained for conventional magnetohydrodynamic flows where the order of magnitude of $\mathbf{J}$ is same as that of $\mathbf{V}\times\mathbf{B}$. In the present study, it is assumed that $\mathbf{J} \gg \mathbf{V}\times\mathbf{B}$ and hence the conventional definition of Hartmann number may not be valid. Therefore, Hartmann number is defined as $Ha = (J_0 L^2/\nu)\sqrt{\mu/\rho_0}$ for the present study. The Hartmann number is the square root of the ratio of the electromagnetic body force to viscous force while the ratio Ra/Pr is the ratio of the gravitational body force to viscous force. Thus, $Ha^2 Pr/Ra$ is the ratio of the electromagnetic body force to the gravitational body force.

2.3. Heat transfer

Assuming negligible viscous heat dissipation, the differential thermal energy balance equation may be expressed as

$$\rho C_p(\mathbf{V}\cdot\nabla T) = k\nabla^2 T + \frac{1}{\sigma}\mathbf{J}\cdot\mathbf{J} \tag{29}$$

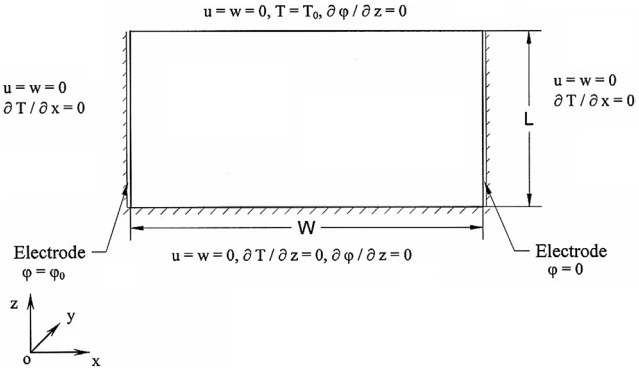

Fig. 1. Computational domain with coordinate system.

which can be non-dimensionalised to obtain

$$\left(\widetilde{\mathbf{V}}\cdot\widetilde{\nabla}\widetilde{T}\right) = \frac{1}{Pr}\widetilde{\nabla}^2\widetilde{T} + \frac{2}{Pr}\widetilde{\mathbf{J}}\cdot\widetilde{\mathbf{J}} \tag{30}$$

The last term on the right of Eq. (30) represents the volumetric heat generation due to Joule heating.

2.4. Simplified model equations and boundary conditions

The boundary conditions used in the present study are explained in Fig. 1, which shows the principal dimensions of the computational domain in the x–z plane. In the present study all gradients in the y-direction are neglected. Further, the electrode pair is assumed to be isopotential surfaces with an externally applied potential difference of φ_0 across them. Rest of the boundaries is assumed to be electrically insulated. All the boundaries of the pool are solid–fluid interfaces, which can be treated as no-slip and no-penetration type such that velocity components are zero at these boundaries. The upper boundary of the liquid pool is an isothermal surface while the rest of the boundaries are assumed to be thermally insulated. The governing equations discussed earlier can be simplified to suit the above conditions as

$$\frac{d^2\tilde{\varphi}}{d\tilde{x}^2} = 0 \tag{31a}$$

$$\widetilde{J}_x = -a\frac{d\tilde{\varphi}}{d\tilde{x}} \tag{31b}$$

$$\widetilde{B}_y[\tilde{x},\tilde{z}] = \frac{1}{2\pi}\int_0^1\int_0^a \frac{-(\tilde{z}-\tilde{z}')\widetilde{J}_x[\tilde{x}',\tilde{z}']}{(\tilde{x}-\tilde{x}')^2 + (\tilde{z}-\tilde{z}')^2}\,d\tilde{x}'\,d\tilde{z}' \tag{31c}$$

$$\frac{\partial\tilde{u}}{\partial\tilde{x}} + \frac{\partial\tilde{w}}{\partial\tilde{z}} = 0 \tag{31d}$$

$$\tilde{u}\frac{\partial\tilde{u}}{\partial\tilde{x}} + \tilde{w}\frac{\partial\tilde{u}}{\partial\tilde{z}} = -\frac{\partial\tilde{p}}{\partial\tilde{x}} + \frac{\partial^2\tilde{u}}{\partial\tilde{x}^2} + \frac{\partial^2\tilde{u}}{\partial\tilde{z}^2} \tag{31e}$$

$$\tilde{u}\frac{\partial\tilde{w}}{\partial\tilde{x}} + \tilde{w}\frac{\partial\tilde{w}}{\partial\tilde{z}} = -\frac{\partial\tilde{p}}{\partial\tilde{z}} + \frac{\partial^2\tilde{w}}{\partial\tilde{x}^2} + \frac{\partial^2\tilde{w}}{\partial\tilde{z}^2} + Ha^2\tilde{J}_x\tilde{B}_y + \frac{Ra}{Pr}\widetilde{T} \tag{31f}$$

$$\tilde{u}\frac{\partial\widetilde{T}}{\partial\tilde{x}} + \tilde{w}\frac{\partial\widetilde{T}}{\partial\tilde{z}} = \frac{1}{Pr}\left[\frac{\partial^2\widetilde{T}}{\partial\tilde{x}^2} + \frac{\partial^2\widetilde{T}}{\partial\tilde{z}^2}\right] + \frac{2}{Pr}\widetilde{J}_x^2 \tag{31g}$$

The corresponding boundary conditions can be expressed as

$$\tilde{\varphi} = 1 \qquad \text{for } \tilde{x} = 0,\ 0 \leqslant \tilde{z} \leqslant 1 \tag{32a}$$

$$\tilde{\varphi} = 0 \qquad \text{for } \tilde{x} = a,\ 0 \leqslant \tilde{z} \leqslant 1 \tag{32b}$$

$$\tilde{u} = \tilde{w} = 0 \qquad \text{for } \tilde{x} = 0,\ 0 \leqslant \tilde{z} \leqslant 1$$
$$\tilde{x} = a,\ 0 \leqslant \tilde{z} \leqslant 1$$
$$\tilde{z} = 0,\ 0 < \tilde{x} < a$$
$$\tilde{z} = 1,\ 0 < \tilde{x} < a \tag{32c}$$

$$\widetilde{T} = 0 \qquad \text{for } \tilde{z} = 1,\ 0 \leqslant \tilde{x} \leqslant a \tag{32d}$$

$$\frac{\partial \widetilde{T}}{\partial \tilde{x}} = 0 \qquad \text{for } \tilde{x} = 0,\ 0 \leqslant \tilde{z} < 1$$
$$\tilde{x} = a,\ 0 \leqslant \tilde{z} < 1 \tag{32e}$$

$$\frac{\partial \widetilde{T}}{\partial \tilde{z}} = 0 \qquad \text{for } \tilde{z} = 0,\ 0 < \tilde{x} < a \tag{32f}$$

3. Numerical solution

The transport equations describing the balance of electric charge, momentum and heat were discretized using the control volume based finite difference method of Patankar [9]. For this, the diffusion terms in the governing equations were approximated by the standard central difference scheme while the convection terms were approximated by the power-law scheme. The discretized equations were iteratively solved using a line-by-line method coupled with the tri-diagonal matrix algorithm. The SIMPLE algorithm was used to handle the pressure-velocity coupling.

The self-induced magnetic flux density $\widetilde{B}_y$ was determined by numerically integrating Eq. (31c) employing mid point method. Special care was taken to evaluate the above integral numerically, since the integrand is singular when $(\tilde{x}, \tilde{z}) = (\tilde{x}', \tilde{z}')$. Since the contribution of a given control volume to the total value of $\widetilde{B}_y$ at the node corresponding to the same control volume is small, the numerical integration was carried out excluding the cell for which $(\tilde{x}', \tilde{z}') = (\tilde{x}, \tilde{z})$ to avoid singularity conditions.

The computer program was benchmarked using results obtained by Emara and Kulacki, who carried out a numerical investigation of thermal convection in a heat-generating fluid layer [10]. They obtained finite difference solutions of the equations governing two-dimensional thermal convection driven by uniform volumetric energy sources distributed in an incompressible fluid ($Pr = 6.5$) in a rectangular enclosure, bounded by an isothermal top boundary and remaining adiabatic boundaries. The computed average Nusselt number obtained using a uniform grid of size 60×30, shows a relative difference of 5.6% for $Ra = 5 \times 10^4$ when compared with the heat transfer correlation of Emara and Kulacki. It is believed that this difference is acceptable as the numerical results are compared with the correlation which was developed for a wide range of Rayleigh number (5×10^3–5×10^8), most of which is in the turbulent flow regime. Experimental measurement of Kulacki and Emara [11] reported an average bottom temperature of 0.3 for a layer of water with large horizontal extent when the Rayleigh number is 2.85×10^5. Present code predicted a horizontally averaged valued of 0.2703 at the bottom layer of water with a finite aspect ratio ($a = 2$). The deviation from the experimental value can be attributed to the differences between the experimental conditions and model assumptions such as constant physical properties, aspect ratio and method of averaging the local temperatures. Present computer program was also successfully benchmarked using the results of Ben Hadid et al. [12], who performed numerical study to investigate the flow structures and the nature of convective regimes in a differentially heated rectangular cavity filled with an electrically conducting liquid metal when it is subjected to a constant vertical magnetic field.

Based on the grid sensitivity analysis, a uniform grid of size 120×60 was employed throughout the present study in order to obtain the numerical solution of the governing partial differential equations.

4. Results

The natural convection in a Joule-heated liquid pool is driven by the gravitational body force and/or the electromagnetic body force that prevail in the system. The electromagnetic body force can be neglected for relatively small values of the Hartmann number. In such thermally driven flows, the convective heat transport in the liquid pool is characterised by the Rayleigh number. On the other hand, in liquids with high electrical conductivity, electromagnetically driven flows prevail by virtue of strong electromagnetic body forces. In such electromagnetically driven flows, the convective heat transport in the liquid pool is characterised by the Hartmann number and the Prandtl number. When both the gravitational body force and the electromagnetic body force are equally strong, the flow pattern and thermal field in a Joule-heated liquid pool strongly depend on the interaction of the gravitational force and the electromagnetic body force. The convective heat transfer is either enhanced or suppressed depending upon whether these two body forces are assisting or opposing each other. Convective behaviour of thermally driven flows, electromagnetically driven flows and combined flows in uniformly Joule-heated liquids are discussed in the following sections.

4.1. Thermally driven flows

Eq. (31a) can be solved analytically for the boundary conditions (32a) and (32b) to get $\widetilde{J}_{\tilde{x}} = 1$, which give rise to a uniform Joule heat generation in the liquid pool. For an infinite horizontal thin layer of liquid with uniform internal heat generation, linear stability theory shows that the onset of motion occurs at $Ra_c = 1386$ [13]. In presence of lateral boundaries, the critical Rayleigh number is expected to be

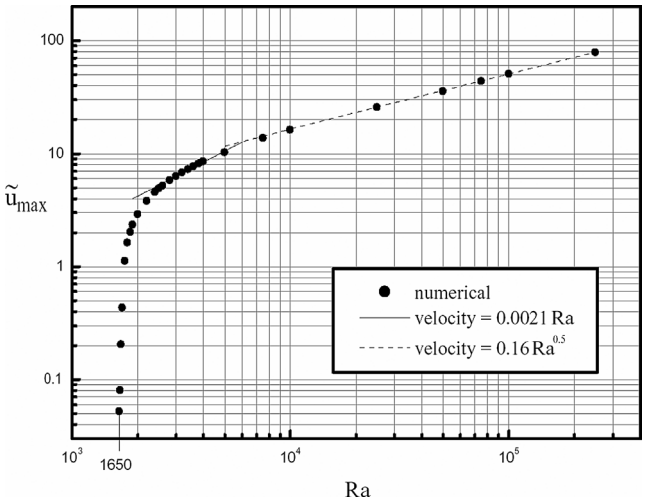

Fig. 2. Maximum horizontal velocity for thermally driven flows ($Pr = 1$).

a function of the aspect ratio. For the present case, liquid is bounded by two lateral walls in the x-direction. These vertical walls suppress the destabilising forces and as a result the critical Rayleigh number is expected to be higher than 1386. The effect of lateral wall for the current aspect ratio ($a = 2$) on the critical Rayleigh number can be illustrated by plotting the maximum horizontal velocity as a function of *Ra* near the instability region. Maximum horizontal velocity against *Ra* for $Pr = 1$ is plotted in Fig. 2. The onset of motion occurs close to $Ra = 1650$ for an aspect ratio of 2. Fig. 2 shows that the maximum horizontal velocity varies linearly with the Rayleigh number soon after the onset of motion. Near the onset of motion, the flow is weak and it is reasonable to equate the gravitational body force to the viscous force which leads to the linear relationship observed. Further, when the flow becomes strong enough, the gravitational body force can be equated to the inertial force such that square of the maximum horizontal velocity varies linearly with the Rayleigh number as seen in Fig. 2. Steady-state solutions could not be obtained for $Ra > 2.5 \times 10^5$.

Flow pattern and isotherms obtained for $Ra = 10^5$ and $Pr = 1$ are shown in Fig. 3. It reveals that the flow field consists of two counter-rotating flow cells, with an upward flow at the centre of the pool and a downward flow near the boundaries. Numerical results obtained for different *Ra* shows that the flow field is relatively stronger at the pool centre for low Rayleigh numbers. As *Ra* increases, the down-flow near the walls becomes stronger than the central up-flow and the centres of the flow cells move towards the bottom corners. Predicted isotherms show that, on any horizontal plane within the liquid pool, the boundaries are relatively cooler than the centre which is consistent with the flow patterns observed.

Horizontally averaged liquid-temperature is plotted in Fig. 4 as a function of $\tilde{z}$ for different values of *Ra*. A constant temperature gradient of -2 at the liquid surface, irrespective of the Rayleigh number, indicates that the steady-state heat transfer rate matches the heat generation rate in the liquid.

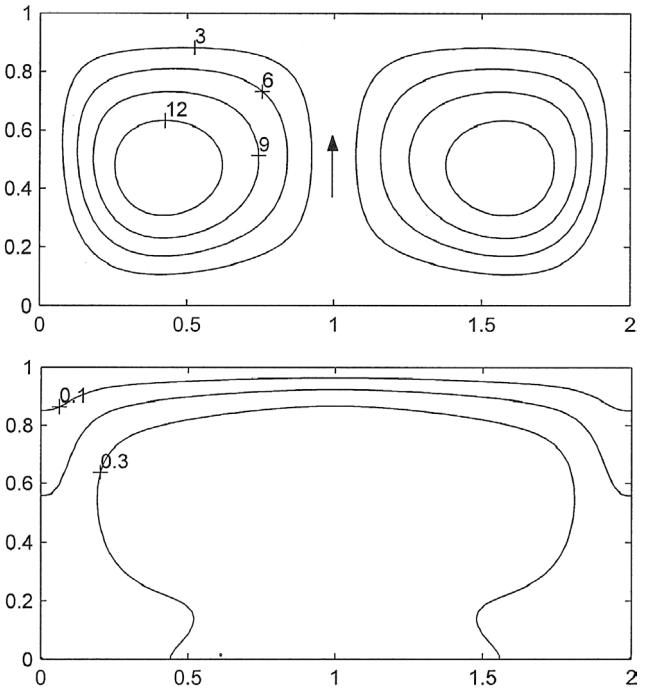

Fig. 3. Contour maps of stream function and isotherms for thermally driven flow ($Ra = 10^5$, $Pr = 1$).

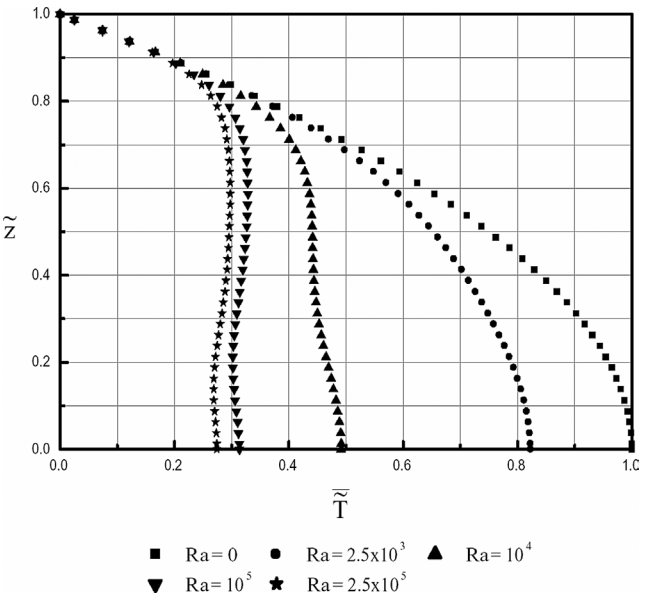

Fig. 4. Horizontally averaged temperature profiles for thermally driven flows ($Pr = 1$).

However, the mean temperature difference across the liquid layer decreases with increase in *Ra*. An average Nusselt number, in terms of the mean temperature difference across the liquid layer, can be defined as

$$Nu_{avg} = \frac{2}{\bar{\bar{T}}_{\tilde{z}=0} - \bar{\bar{T}}_{\tilde{z}=1}} = \frac{2}{\bar{\bar{T}}_{\tilde{z}=0}} \tag{33}$$

where $\bar{\bar{T}} = \frac{1}{a}\int_0^a \tilde{T}\,\mathrm{d}\tilde{x}$ is the horizontally averaged temperature of the liquid.

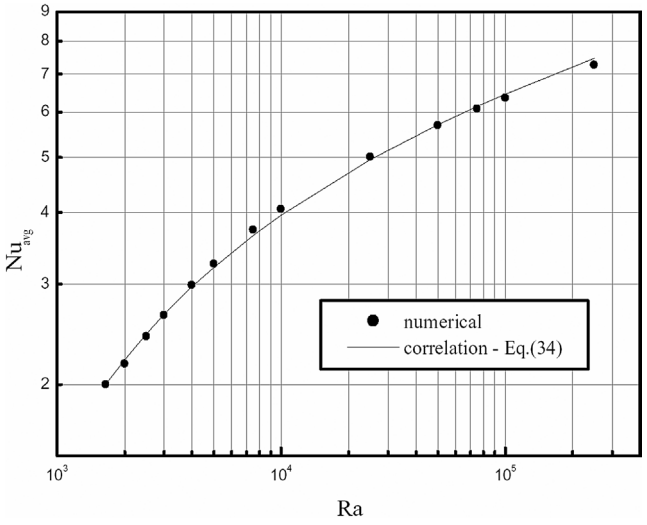

Fig. 5. Average Nusselt number for thermally driven flows ($Pr = 1$).

Fig. 4 implies that $Nu_{\text{avg}} = 2$ for conduction, i.e. when Rayleigh number is less than the critical value, $Ra = 1650$. Convection currents in the post stability regime lower the mean temperature difference across the liquid layer as illustrated in Fig. 4. This results in an increase in Nu_{avg}. Thus, Nu_{avg} is an indication of degree of convection in the post stability regime. The average Nusselt number for $Pr = 1$ is plotted as a function of Ra in Fig. 5. Based on the results obtained, an empirical correlation was developed for Nu_{avg} as given by Eq. (34).

$$Nu_{\text{avg}} = 2 + 2.5 \log\left(\frac{Ra}{1650}\right)$$

$$\text{for } 1650 \leqslant Ra \leqslant 2.5 \times 10^5 \text{ and } Pr = 1 \qquad (34)$$

The correlation (34) gives a maximum relative error of 2.8% and an rms value of 1.6% when compared with the Nu_{avg} computed. The functional form of the above correlation leads to $Nu_{\text{avg}} = 2$ at the critical Rayleigh number ($Ra = 1650$).

4.2. Electromagnetically driven flows

The governing partial differential equations show that the electric field, flow field and thermal field are decoupled for magnetohydrodynamic flows for low magnetic Reynolds number when physical properties are assumed to be temperature independent. Therefore, unlike in the case of thermally driven flows where the flow and thermal fields are intimately coupled, in electromagnetically driven flows, the flow field can be obtained for a given Hartmann number and the thermal field can be obtained subsequently for the computed flow field.

Fig. 6 presents the magnetic flux density ($\widetilde{B}_y$) contours given by Eq. (31c). The current density $\widetilde{J}_x$ results in the magnetic flux density $\widetilde{B}_y$ and the interaction of the two results in the electromagnetic body forces, $\widetilde{J}_x \widetilde{B}_y (= \widetilde{B}_y$ for $\widetilde{J}_x = 1)$ which act in the z-direction. The electromagnetic

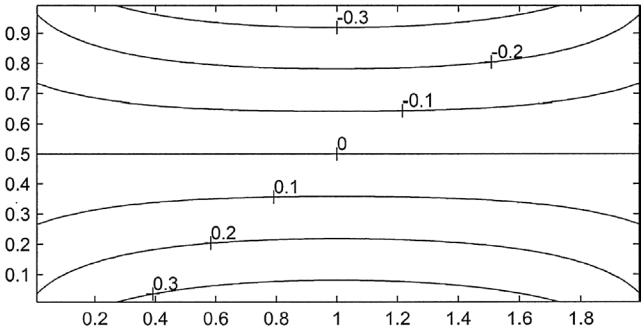

Fig. 6. Contour map of y-component of magnetic flux density.

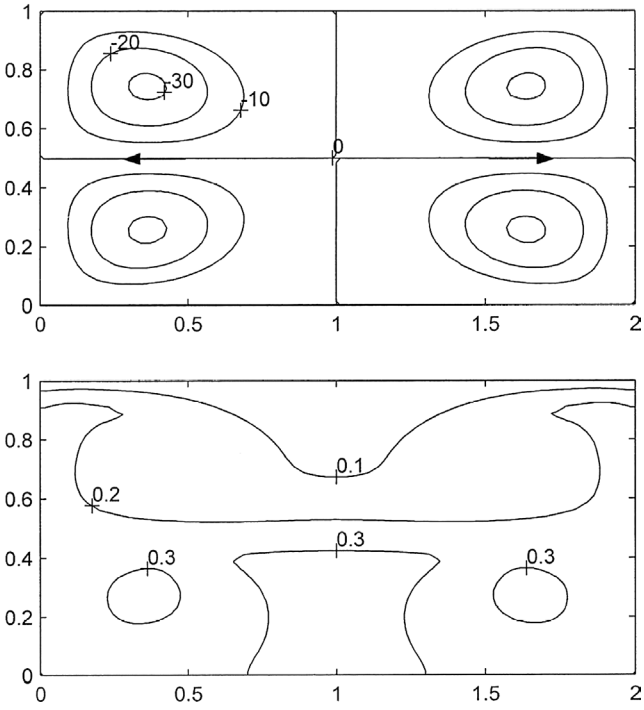

Fig. 7. Contour maps of stream function and isotherms for electromagnetically driven flow ($Ha^2 = 2 \times 10^6$, $Pr = 1$),

body forces try to pull the liquid towards the mid-height of the pool. It is also evident from Fig. 6 that the contracting forces are maximum at the centre of the horizontal boundaries. The non-uniform electromagnetic body force due to the self-induced magnetic field result in magnetohydrodynamic flows in the liquid. Fig. 6 suggests a flow pattern with four counterrotating flow cells. The flow pattern and corresponding isotherms for $Ha^2 = 2 \times 10^6$ and $Pr = 1$ are presented in Fig. 7. The numerical results obtained show that size of the flow cells diminishes as Ha^2 increases leaving the pool centre relatively stagnant. Deformation of the isotherms from its conduction solution, which are horizontal lines, can be explained in terms of the direction of the flow cells.

The maximum horizontal velocity obtained for $10^3 \leqslant Ha^2 \leqslant 4 \times 10^7$ is plotted in Fig. 8. It shows two distinct regions with two different slopes. The maximum horizontal velocity varies linearly with Ha^2 for weak flows while it varies linearly with Ha for strong flows. These observa-

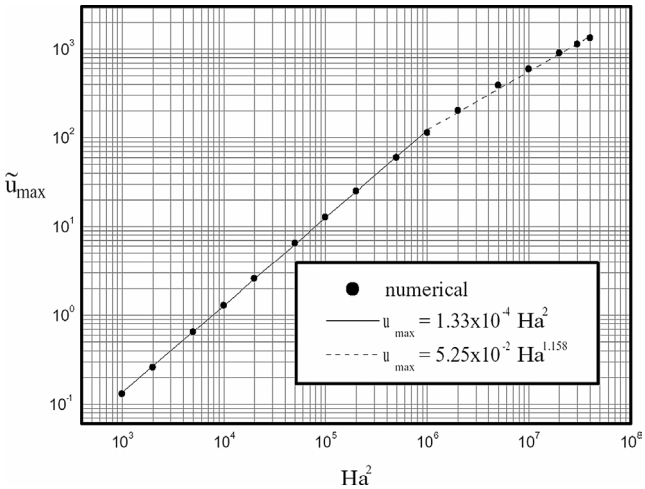

Fig. 8. Maximum horizontal velocity for electromagnetically driven flows.

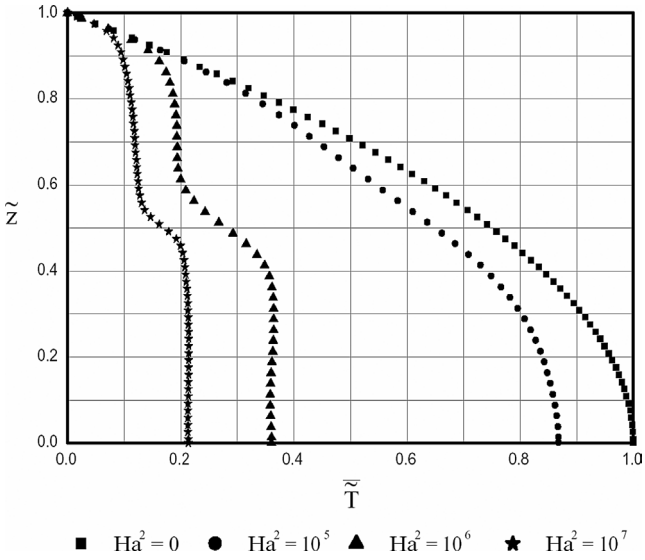

Fig. 9. Horizontally averaged temperature profiles for electromagnetically driven flows ($Pr = 1$).

tions were verified by equating the electromagnetic body force to the viscous force under weak flow conditions and to the inertial force under strong flow conditions. In the physical modelling study conducted by Choudhary and his co-workers [1] to experimentally measure the electromagnetically driven flow in a horizontally placed trough filled with mercury, they observed that maximum velocity varies linearly with the electrode current. The Reynolds number for their physical model was reported to be in the range of 4×10^4 to 2×10^5. This supports the present observation that the linear relationship is valid for strong flows.

The horizontally averaged temperature profiles for the magnetohydrodynamic flows for $Pr = 1$ are plotted in Fig. 9. The conduction profile is compared with the temperature profiles for the three different values of Ha^2 (i.e., $Ha^2 = 10^5$, 10^6 and 10^7). All these profiles show that the maximum liquid temperature occurs at the adiabatic bottom wall. As

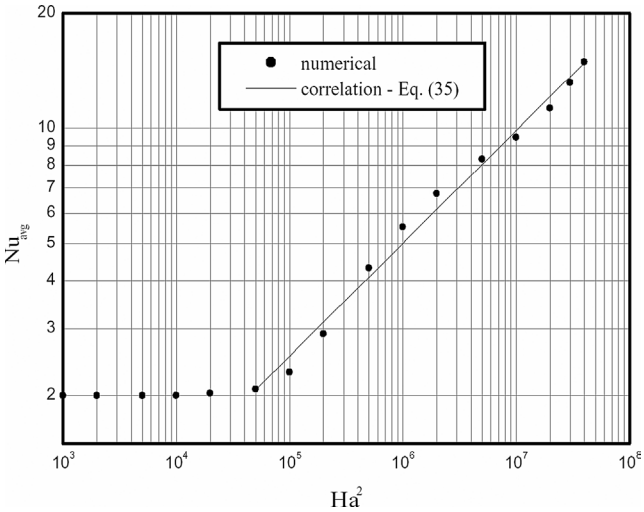

Fig. 10. Average Nusselt number for electromagnetically driven flows ($Pr = 1$).

shown in case of thermally driven flows, the temperature gradient at the pool top equals to -2. In addition, the horizontally averaged temperature profiles exhibit a constant slope of -1 at $\tilde{z} = 0.5$. This is due to the fact that the heat transfer across $\tilde{z} = 0.5$ is purely due to conduction as the vertical velocity component vanishes at $\tilde{z} = 0.5$. Moreover, the heat transfer rate at $\tilde{z} = 0.5$ is half of that at $\tilde{z} = 1$.

The average Nusselt number obtained for Hartmann numbers in the range of $10^3 \leqslant Ha^2 \leqslant 4 \times 10^7$ and $Pr = 1$ are plotted in Fig. 10. Steady-state solutions could not be obtained for $Ha^2 > 4 \times 10^7$. Fig. 10 shows that the effect of convection is not significant for $Ha^2 < 5 \times 10^4$. The heat transfer correlation given by Eq. (35) can be used to predict the average Nusselt number within a maximum relative error of 10.2% and an rms value equal to 6.4%.

$$Nu_{\text{avg}} = 0.085 Ha^{0.59} \quad \text{for } 5 \times 10^4 \leqslant Ha^2 \leqslant 4 \times 10^7 \text{ and } Pr = 1 \tag{35}$$

4.3. Combined effect of Rayleigh and Hartmann numbers

Numerical values of the average Nusselt number obtained for $5 \times 10^3 \leqslant Ra \leqslant 10^5$ and $10^3 \leqslant Ha^2 \leqslant 2 \times 10^7$ with $Pr = 1$ are plotted in Fig. 11. It shows that, for a given Rayleigh number, Nu_{avg} at the liquid surface remains unaffected by the Hartmann number initially as the electromagnetic body force is insignificant in relation to the gravitational body force. As the Hartmann number is increased, the convective heat transfer gets suppressed till the average Nusselt number curve reaches a minimum. The suppression is due to the fact that both the body forces oppose each other near the heat transfer boundary. A total suppression of the flow such that the average Nusselt number approaches its conduction limit does not take place because the counter acting driving forces (i.e., the gravitational body force and the electromagnetic body force) are not identical in all respects. Further increase in the Hartmann number enhances

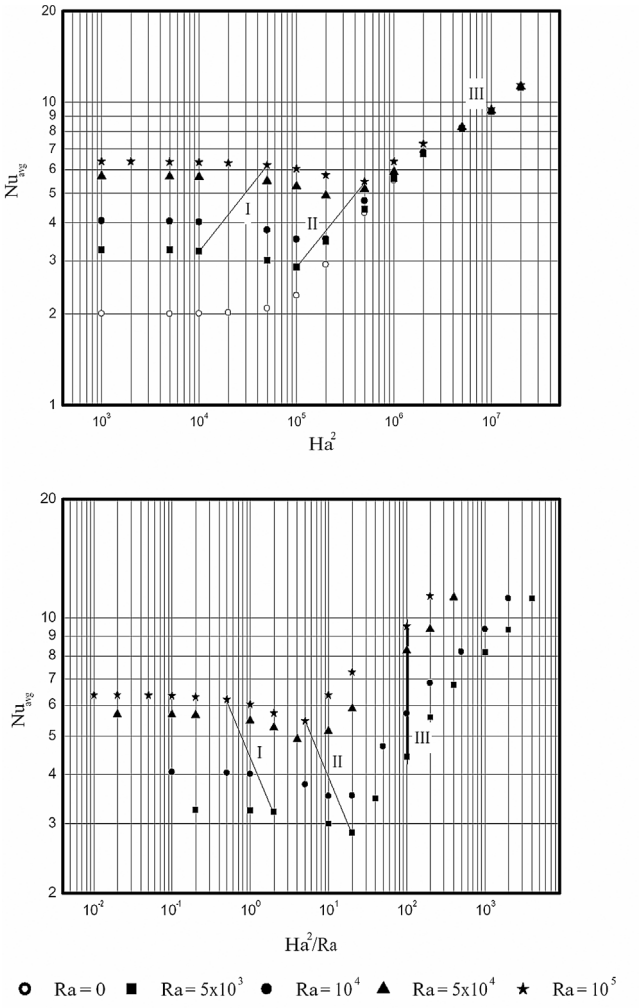

Fig. 11. Average Nusselt number for combined flows ($Pr = 1$).

the convective heat transfer as both the driving forces assist each other in this zone. Finally, the flow field becomes governed by the electromagnetic body force as the gravitational body force becomes insignificant in comparison with the electromagnetic body force. Thus, the average Nusselt number curve exhibits following characteristic points:

(1) *Onset point* at which flow suppression due to the electromagnetically driven flow cells becomes visible. In this zone, the gravitational body force governs the primary flow cells. Effect of Electromagnetic body force can be neglected up to the onset point.
(2) *Transition point* which corresponds to the minimum Nusselt number. At this point, the electromagnetically driven flow cells acquire the same strength as that of the thermally driven flow cells. A flow reversal takes place near the heat transfer boundary soon after the transition point such that the flow cells governed by the electromagnetic body force become the primary flow cells.
(3) *Termination point* where the Nusselt number curve merges with the Nusselt number curve for $Ra = 0$ case. Beyond this point, the gravitational body force can be neglected.

At the transition point, the maximum horizontal velocity caused by gravitational body force can be equated to that caused by the electromagnetic body force. This results in the following relationship for the transition point:

$$\left(\frac{Ha^2}{\sqrt{Ra}}\right)_{\text{transition}} \approx 1200 \quad \text{for } Pr = 1 \text{ and } a = 2 \tag{36}$$

Based on Eq. (36) and Fig. 11, the onset point condition can be defined as

$$\left(\frac{Ha^2}{\sqrt{Ra}}\right)_{\text{onset}} \approx 120 \quad \text{for } Pr = 1 \text{ and } a = 2 \tag{37}$$

Eq. (37) assumes that the onset point occurs when the maximum horizontal velocity due to the electromagnetic body force becomes 10% of the maximum horizontal velocity due to the gravitational body force. Fig. 11 shows that the average Nusselt number becomes independent of Ra when $Ha^2/Ra \approx 10^2$. Therefore, termination point can be expressed as given by Eq. (38). The loci of onset point, transition point and termination point are shown in Fig. 11.

$$\left(\frac{Ha^2}{Ra}\right)_{\text{termination}} \approx 100 \quad \text{for } Pr = 1 \text{ and } a = 2 \tag{38}$$

The flow pattern and isotherms for $Ra = 10^5$, $Ha^2 = 2 \times 10^6$ and $Pr = 1$ are presented in Fig. 12. A comparison with Figs. 3 and 7 clearly shows that both the gravitational and electromagnetic body forces are responsible for the natural convection shown in Fig. 12.

As discussed earlier, the Nu_{avg} curves for the combined flow consist of two regions. In the first region, from onset point to the transition point (i.e., $120 \leqslant Ha^2/\sqrt{Ra} \leqslant 1200$), the heat transfer coefficient decreases with increase in Ha^2/Ra ratio. The heat transfer correlation for the flow suppression zone can be developed based on a rational relationship given by Eq. (39).

$$Nu_{\text{avg}} = Nu_{\text{gravity}}\left(\frac{120\sqrt{Ra}}{Ha^2}\right)^n \quad \text{for } Pr = 1 \text{ and } a = 2 \tag{39}$$

In correlation (39) Nu_{gravity} is the average Nusselt number given by Eq. (34) for thermally driven flow for the given Ra and $n = 0.049 + 2.105 \times 10^{-7} Ra$.

In the second region, from the transition point to the termination point, the heat transfer coefficient increases with increase in Ha^2/Ra ratio. Therefore, the heat transfer correlation for the flow enhancement zone can be obtained as Eq. (40).

$$\text{Nu}_{\text{avg}} = Nu_{\text{Lorentz}}\left(\frac{Ha^2/Ra}{100}\right)^n \quad \text{for } Pr = 1 \text{ and } a = 2 \tag{40}$$

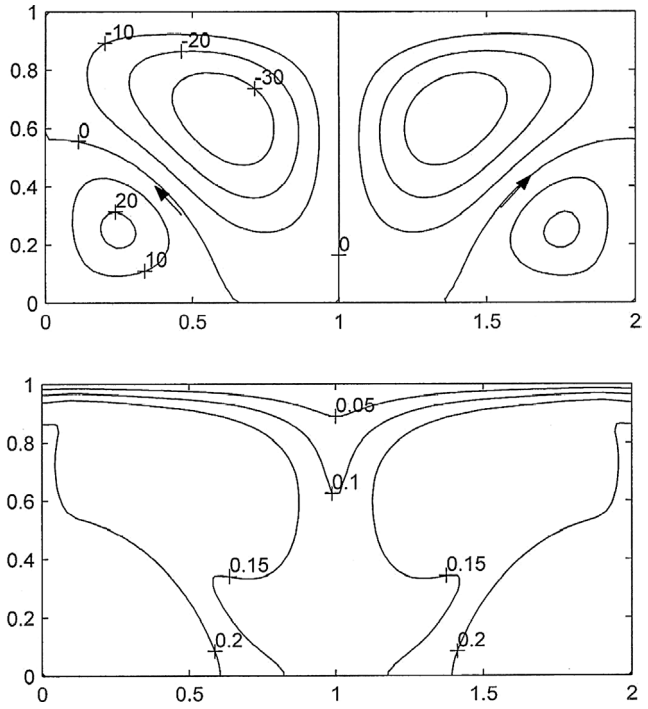

Fig. 12. Contour maps of stream function and isotherms for combined flow. ($Ra = 10^5$, $Ha^2 = 2 \times 10^6$, $Pr = 1$).

where Nu_{Lorentz} is the average Nusselt number given by Eq. (35) for electromagnetically driven flow *at the termination point* and $n = 0.2105 - 1.053 \times 10^{-7} Ra$. Correlations (39) and (40) predict the average heat transfer coefficient within a maximum relative error of 10.5% and an rms value of 2.52%.

4.4. Effect of Prandtl number

Effect of Prandtl number on *thermally driven flows* in a uniformly Joule-heated liquid was investigated by varying Pr in the range of $10 \leqslant Pr \leqslant 10^3$. Results obtained for thermally driven flows showed that the thermal field was unaffected by the Pr for a given Ra.

Effect of Prandtl number on *electromagnetically driven flows* in a uniformly Joule-heated liquid was investigated by varying Pr in the range of $0.01 \leqslant Pr \leqslant 10$. This range was chosen as the electromagnetically driven flow occurs in liquids with high electrical conductivity. Effect of Pr on the heat transfer rate at the pool surface is illustrated in Fig. 13, where Nu_{avg} is plotted as a function of Pr with Ha^2 as the parameter. It is evident from Fig. 13 that, for a given Ha^2, the Nu_{avg} is strongly affected by the Pr. The Nusselt number correlation (35) can be modified as Eq. (41) to account for the effect of Prandtl number. Eq. (41) predicts the effect of Prandtl number within a maximum relative error of 13% and an rms value of 6%.

$$Nu_{\text{avg}} = \max\left(2, 0.085 Ha^{0.59} Pr^{0.4}\right) \quad \text{for } 5 \times 10^4 \leqslant Ha^2 \leqslant 4 \times 10^7 \text{ and } 0.01 \leqslant Pr \leqslant 10 \qquad (41)$$

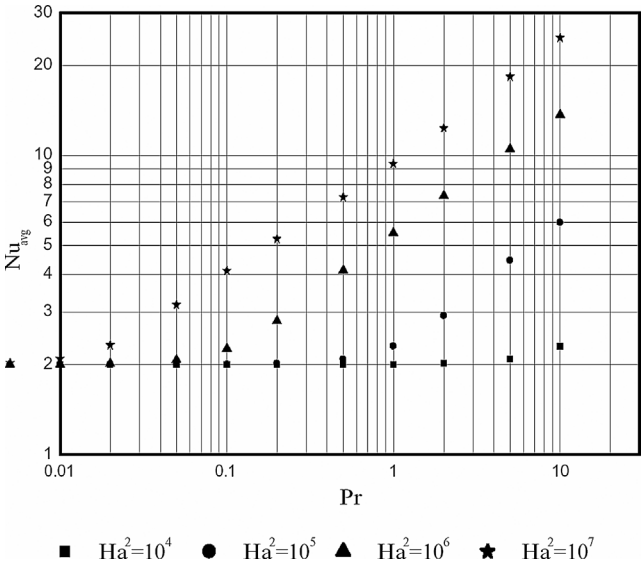

Fig. 13. Effect of Prandtl number on average Nusselt number for electromagnetically driven flows.

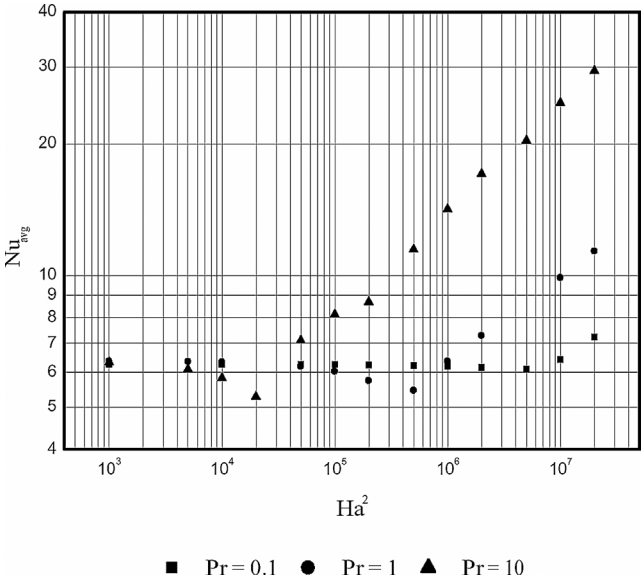

Fig. 14. Effect of Prandtl number on average Nusselt number for combined flows.

The effect of Prandtl number on *combined flows* was studied using three different values of Pr (0.1, 1 and 10) for $Ra = 10^5$ and $10^3 \leqslant Ha^2 \leqslant 2 \times 10^7$. The numerical values of the average Nusselt number obtained are plotted in Fig. 14. The Nu_{avg} versus Ha^2 curves show that both the onset and the transition point occurs at an early stage when the Pr increases for a given Rayleigh number. This is due to the fact that the gravitational body force, which is proportional to Ra/Pr, decreases with increase in Pr for a given Ra. Thus, the $Ha^2 Pr/Ra$ ratio, as expected, indicates the relative strengths of the electromagnetic and the gravitational body forces. Therefore, the findings summarised in Section 4.3 for $Pr = 1$ can be mod-

ified to account for the effect of Prandtl number as follows:

- Electromagnetic body force can be ignored when $Ha^2Pr/\sqrt{Ra} < 120$.
- Gravitational body force can be neglected when $Ha^2Pr/Ra > 100$.
- Natural convection is governed by both electromagnetic body force and gravitational body force when $Ha^2Pr/\sqrt{Ra} > 120$ and $Ha^2Pr/Ra > 100$.
- The Nusselt number curve exhibits a minimum when $Ha^2Pr/\sqrt{Ra} \approx 1200$.

5. Conclusions

Convective behaviour of a uniformly Joule-heated liquid pool in a rectangular cavity, with an aspect ratio of 2, was studied using a two-dimensional mathematical model. Dimensional analysis of the present problem showed that the gravitational body force is characterised by the Rayleigh number (Ra) while the electromagnetic body force is governed by the Hartmann number (Ha). Ha^2Pr/Ra represents the ratio of the electromagnetic body force to the gravitational force prevailing in a Joule-heated liquid pool. These forces result in convection currents in the liquid pool. Other dimensionless numbers governing the natural convection in the Joule-heated liquid pool are the Prandtl number of the liquid (Pr) and the aspect ratio (a) of the cavity. Physical properties of the model fluid were assumed to be constant except for the Boussinesq approximation. Present study leads to the following conclusions:

(1) Thermally driven natural convection prevails in a uniformly Joule-heated liquid pool when $Ha^2Pr/\sqrt{Ra} < 120$. For thermally driven flows, the thermal field is unaffected by Pr when $10^3 \geqslant Pr \geqslant 10$.
(2) Electromagnetically driven flows occur in a uniformly Joule-heated liquid pool when $Ha^2Pr/Ra > 100$. The magnetohydrodynamic flow is independent of the Pr while the thermal field for a given flow is strongly modified by Pr.
(3) Natural convection is governed by both electromagnetic body force and gravitational body force when $Ha^2Pr/\sqrt{Ra} > 120$ and $Ha^2Pr/Ra > 100$. The Nu_{avg} curve in the case of combined flows exhibit three characteristic points, viz., onset point, transition point and termination point.
(4) The Nusselt number curve exhibits a minimum when $Ha^2Pr/\sqrt{Ra} \approx 1200$.
(5) Empirical correlations were developed for average Nusselt number for thermally driven, electromagnetically driven and combined flows in a uniformly Joule-heated liquid pool in a rectangular cavity.

Acknowledgements

The authors would like to express their deepest appreciation to Prof. S. Ghosh Moulic, Department of Mechanical Engineering, Indian Institute of Technology, Kharagpur, India, for his valuable help and useful discussions on electromagnetically driven flows.

References

[1] M. Choudhary, J. Szekely, B.I. Medovar, Yu.G. Emelyanenko, The velocity field in the molten slag region of ESR Systems: A comparison of measurements in a model system with theoretical predictions, Metall. Trans. B 13 (1982) 35–43.
[2] Y.M. Ferng, C.C. Chieng, C. Pan, Numerical simulations of electroslag remelting process, Numer. Heat Transfer A 16 (1989) 429–449.
[3] M.J. Austin, D.E. Bourne, A mathematical model of an electric glass furnace, Glas. Tech. 14 (1973) 78–84.
[4] M.K. Choudhary, A three-dimensional model for flow and heat transfer in electrical glass furnaces, IEEE Trans. Indust. Appl. IA 22 (1986) 912–921.
[5] H. Igarashi, T. Takahashi, Three-dimensional mathematical model for an electric glass melter used to vitrify nuclear high level liquid wastes, Glas. Tech. 32 (1991) 206–216.
[6] R.P. Feynman, The Feynman Lectures on Physics II, Narosa Publishing House, 1992.
[7] I. Stakgold, Green's Functions and Boundary Value Problems, Wiley, New York, 1979.
[8] P.H. Roberts, An Introduction to Magnetohydrodynamics, Longman, London, 1967.
[9] S.V. Patankar, Numerical Heat Transfer and Fluid Flow, McGraw-Hill, New York, 1980.
[10] A.A. Emara, F.A. Kulacki, A numerical investigation of thermal convection in a heat-generating fluid layer, ASME J. Heat Transfer 102 (1980) 531–537.
[11] F.A. Kulacki, A.A. Emara, Steady and transient thermal convection in a fluid layer with uniform volumetric energy sources, J. Fluid Mech. 83 (1977) 375–395.
[12] H. Ben Hadid, D. Henry, S. Kaddeche, Numerical study of convection in the horizontal Bridgman configuration under the action of a constant magnetic field—two-dimensional flow, J. Fluid Mech. 333 (1997) 23–56.
[13] F.A. Kulacki, R.J. Goldstein, Thermal convection in a horizontal fluid layer with uniform volumetric energy sources, J. Fluid Mech. 55 (1972) 271–287.